# P and SV waves 3-D Numerical Modeling of AVOA from Heterogeneous Fractured Reservoirs

Xiang Zhu, Feng Shen, M. Nafi Toksöz
Earth Resources Laboratory
Massachusetts Institute of Technology

## ABSTRACT

We study the effects of fracture-induced anisotropy and lateral fracture density heterogeneity on the reflected P and SV wave amplitude variation with offset and azimuth (AVOA), using 3-D finite-difference simulations. The models show that for an isotropic layer overlying on a fractured reservoir, the anisotropic behavior of AVOA depends on fracture density as well as the contrast in elastic properties between the reservoir layer and the overlying material. It is also verified that the SV wave is more sensitive to fractures than the P wave. The sensitivity of AVOA to spatial variations of fracture density is also investigated.

## INTRODUCTION

Seismic reflection amplitude versus offset (AVO) conventionally serves as a hydrocarbon indicator, particularly for gas accumulations. A medium containing vertical fractures is anisotropic, which may cause azimuthal variations in AVO responses. This anisotropic behavior of the AVO response can be used to derive the properties of the fractured medium. To accomplish this, a thorough understanding of the effects of fractures on reflection amplitude as a function of source-receiver offset and azimuthal angle (AVOA) is very important.

One way to calculate the AVOA is to solve the anisotropic Zoeppritz equations analytically. (Rüeger and Tsvankin, 1995, Thomsen, L., 1993, Teng, 1996, Li, 1996) Due to the complexity of these equations, approximations are made in deriving the explicit solutions, which are based on assumptions of small velocity contrasts, small source-receiver offsets, and weak anisotropy. These solutions also assume that the seismic wavelength is much smaller than the heterogeneity scale at the reflecting horizon. In order to avoid some of these assumptions and to investigate the effect of heterogeneity, we use a 3-D elastic finite-difference program to simulate wave propagation and AVOA behavior in fractured reservoirs.

The simplest type of anisotropy, transverse isotropy (TI), is generated when parallel fracture planes are introduced into an originally isotropic background rock. When the fracture planes are vertical, the symmetry axis is horizontal, resulting a type of anisotropy called horizontal transverse isotropy (HTI). We focus our study on the AVOA responses of HTI media in order to better understand the effect of anisotropy on AVOA, the sensitivity of P and SV wave reflections to the presence of fractures, and the effects of fracture density heterogeneity on AVOA behavior.

To determine AVOA of a homogeneous fractured medium, we build a series of two-layer models. In each model, the upper layer is isotropic so that the reflected signals contain only P and SV waves. The lower layer is horizontal transversely isotropic material, with the x axis as its symmetry axis. This lower layer is formed by introducing vertical fractures into an originally isotropic background medium. The calculations of the elastic constants of this layer from the fracture parameters are based on the effective medium models developed by Hudson (1981, 1990, 1996a, 1996b).

An explosive source emits P wave from the surface. Since the overburden is isotropic, there is only a P wave propagating downward. After the wave reaches the interface, the transmitted energy propagates downward as a qP wave, a S1 wave (fast) and a S2 wave (slow) in the HTI layer, while the reflected energy propagates upward in the forms of a P wave, a SV wave and a SH wave in the isotropic overburden. We restrict our study on P and SV waves because the energy of SH wave is minimal in our case. Taking full advantage of 3-D numerical simulation, we record the seismograms over the entire surface, instead of setting up only separated receiver lines. Therefore, we obtain a bitmap of the reflected waves at every surface grid position.

# HOMOGENEOUS FRACTURED MEDIUM

We first focus on studying the effects of anisotropy by keeping the fracture density constant. Therefore, the reflecting layer is a homogeneous HTI medium. For a homogeneous medium, the bitmap of reflection data from one shot contains the full AVOA response.

In a HTI medium, the velocities of the P and SV waves are functions of the azimuthal angle $\phi$, where $\phi$ is defined as the angle between the incident plane and the symmetry axis of the medium (the x axis in this study). When $\phi = 90°$, the incident plane is parallel to fracture planes, and the particle motions of the P and SV waves are restricted to this plane. In this case, there is no interaction between the waves and the fractures, and the seismic velocities are the same as in isotropic case. This is the fast wave direction. As $\phi$ decrease, particle motions start to intersect the fracture planes, reducing the propagation velocities. At $\phi = 0°$, the incident plane is normal to the fracture strike, the particlemotions are normal to the fractures, and the propagation velocities are at their lowest. This is called the slow wave direction.

Only the horizontal components of particle motion are affected by fractures. Within the offset range of our models, most of the P wave energy is in vertical oscillation, while most of the SV wave energy is in horizontal oscillation. Therefore, the SV wave should be more sensitive to fractures than the P wave.

To view AVOA of the models, we use colormaps of the reflected amplitudes at the surface. The amplitude of the reflected signal is a 2-D function of the receiver position (x,y). These colormaps in (x,y) space directly show the reflection strength as a function of offset and

azimuth, so there is no need to convert them into (offset, azimuth) space. The lateral position of any reflecting point on the interface is (x/2,y/2), that is, mid point between the source at (0.0) and the receiver at (x,y). To see the quantitative magnitude of reflection variation with offset, we also plot the reflected amplitude as the function of source-receiver distance along the $\phi = 0°, 45°, 90°$ azimuth directions. These curves can be considered to be AVO curves, except that the coordinate is twice the CDP offset.

The degree of anisotropy in AVOA depends on the fracture density. Figure 1 shows the colormaps of AVOA responses and AVO curves for models with varying fracture density. All models have the same overburden properties. The HTI layers are generated by introducing gas-filled fractures into the same isotropic background. When the fracture density is zero, the model is isotropic. We expect the AVOA response to also be isotropic. This is supported by the results (1a) where the pattern of colormap of the AVOA response is circular, showing no azimuthal dependence. The AVO curves at 0, 45 and 90 degrees also coincide. As the fracture density increases, the medium becomes anisotropic, and the AVOA response reflects this change. Along the fast wave direction ($\phi = 90°$), the AVO response is the same as in isotropic case because the wave propagates at the same velocity. But in all other directions, the AVO response deviates from the isotropic case. As $\phi$ decreases, AVO deviates more from isotropic case, and at $\phi = 0°$, the slow wave direction, the deviation is strongest. If we define the degree of anisotropy of AVOA as the deviation of AVO at $\phi = 0°$ from that at $\phi = 90°$, the dependence of anisotropic behavior of AVOA on fracture density is approximately linear. The above is true for both the P and SV waves.

Comparing the AVOA responses of the P and SV waves in Figure 1, we see that the SV wave demonstrates stronger anisotropy. It is because that the SV wave interacts more with the fractures.

It is also interesting to note that the reflection pattern is not really elliptic, although it appears to be. In fact, its azimuthal dependence is a superposition of $\cos^2 \phi$ and $\cos^4 \phi$ terms. Banik (1987) showed a velocity plot as the function of the azimuth, which displayed very similar pattern.

The reflecting layers in the above models are based on an isotropic background material which yields significant anisotropic AVOA behavior when fractures are introduced. For some background material, however, anisotropic AVOA behavior is not visible when fractures are introduced. Sayers and Rickett (1997) showed that for three models of Class 1, 2 and 3 gas sands, there is no visible anisotropy in P wave reflection amplitude within 30 degree incident angle.

For comparison with their results, we performed the same calculation for two different background models, in which the 10% fracturing is introduced to the second layers. The AVOA colormaps and AVO curves for these models are shown in Figure 2. Figure 2a is the colormap of the P wave AVOA response for model 1. It appears that the reflection pattern is circular with no visible azimuthal dependence. Figure 2c shows the AVO curves at 0, 45 and 90 degree azimuths for this model. The three curves coincide. For this model, there is no

obvious anisotropic behavior in the P wave reflection amplitudes, even though the reflecting layer is anisotropic. Figure 2b shows the colormap of the P wave AVOA for model 2. In this case, the reflection pattern is elliptical, indicating that the medium anisotropy produces clear anisotropic behavior in the P wave reflection amplitudes. Figure 2d shows its AVO curves at azimuths of 0, 45 and 90 degrees. In this case we see significant azimuthal variation in the AVO response.

Model 1 has large velocity contrast between the two layers. The AVO effect for this model is strong. Although the second layer is anisotropic, the perturbation of anisotropy on the isotropic background is relatively quite weak. Therefore, the anisotropic behavior of AVOA is not clearly seen. In model 2, however, the velocity contrast between the two layers is much smaller. The reflection strength is much less, but the anisotropy in the reflection amplitude is clearly observed. These results indicate that the degree of anisotropy strongly depends on the contrast of elastic properties at the reflecting interface.

# FRACTURE DENSITY HETEROGENEITY

In this section we investigate the effect of fracture density heterogeneity on AVOA behavior. The reflecting surface is kept flat, and the fracture alignment is fixed at 90°. The fracture density varies only laterally. Therefore, the medium is HTI with a fixed symmetry axis and laterally varying strength of anisotropy. As mentioned before, when the incident plane of waves is normal to the fracture strike (i.e., $\phi$ is small), the fractures exert stronger effects on the reflection amplitudes. It follows that the fracture density heterogeneity perturbation has a maximum effect for $\phi = 0°$, and the effect decreases as $\phi$ is approaching 90°. As in the case of a homogeneous fracture density model, the AVO response is the same as for an isotropic (non-fractured) model when $\phi = 90°$. We build a series of test models to examine the effects of heterogeneity in fracture density on AVOA. In the models the mean fracture density is 10% with variations of ±5%. The fracture density varies as either a smooth cosine function or a certain type of stochastic function. The AVOA of the model with constant 10% fracture density yields smooth near-elliptical pattern (see Column 3 in Figure 1). The AVOA of the heterogeneous models can be considered as a perturbation on this background.

Figure 3 shows the results for the first test model. In this model, the fracture density varies as $10\% + 5\%\cos(2\pi x/160m)$. The period of this variation, 160 m, is roughly 1.5 wavelength of P wave. This type of variation produces a pattern of vertical lines, as shown in Figure 3a. This figure is actually just a windowed colormap of the model, in which only the reflecting area of the surface is shown. In this model, the fracture density varies only in the slow wave direction. Therefore, as the incident plane rotates from the slow wave direction to the fast wave direction, the heterogeneity scale (or the correlation length) varies from 160 m to infinity. This model enables us to observe the sensitivity of AVO to various correlation lengths of the heterogeneity.

The reflection pattern of the P waves of this model appears almost indistinguishable from that of the homogeneous model with 10% fracture density (Figure 3b and Figure 1). This implys that the perturbation is small. The AVO curves (Figure 3c) are also very close to those for the homogeneous case. To see if heterogeneity has any effect on AVOA, we subtract the AVOA for the homogeneous 10% fractured medium from the AVOA of this heterogeneous case. The residue then shows a clear vertical-line pattern (with some distortion) (Figure 3e), which is closely related to the model heterogeneity pattern (Figure 3a). Therefore, heterogeneity in fracture density does perturb the AVOA, but the effect is smaller than that of the mean anisotropy. Figure 3f shows the curves of AVO residue at $\phi = 0$, 45, and 90 degrees. It should be noted that the vertical scale of this plot is one order of magnitude smaller than that of the AVO plot (Figure 3c).

Without using the AVOA of the homogeneous fracture density model as a reference, the heterogeneity perturbation can also be determined by using Shuey's equation along any receiver line. Figure 3.(d) is the plots of AVO in Shuey's two-term approximation (i.e., $A + B\sin^2\theta$) at $\phi = 0°, 45°, 90°$, with A and B determined by best-fitting the model AVO curves using Shuey's equation. The AVO residues obtained by subtracting the Shuey curves from the model results also provide heterogeneity information (Figure 3g). Since no homogeneous background AVOA information is available for processing real data from the field, using the Shuey equation as a reference is a realistic way of obtaining the heterogeneity estimates. From homogeneous case we find that the AVO curves match Shuey's equation very well up to the incident angle of 25 degrees. For higher angles, the deviation becomes significant because Shuey's equation ignores higher order terms. The AVO residue results (Figure 3g) are distorted by this mismatch beyond 25 degrees.

The AVOA for the P-SV wave is much more sensitive than that of the P-P wave. Its AVOA colormap is strongly perturbed by the same heterogeneity distribution (Figure 3h). After removing the homogeneous AVOA background, the residue forms a quite clear image of the model heterogeneity pattern. The relative scale of residue is also much lager than that for the P-P wave. This is explained by the greater sensitivity of shear waves to the presence of fractures. The wavelength of the SV wave is smaller than that of the P wave, which also contributes to the better resolution.

Figure 4 shows the results for a similar model, in which the correlation scale of the perturbation is half of that in the first model. In this case, the P wave residue (Figure 4e) no longer shows a clear pattern of the model heterogeneity, whereas that of the SV wave still yields a very good image (Figure 4j).

Figure 5 shows the results for a model where the fracture density heterogeneity varies as a cosine function of the source-receiver separation. Figure 5a is the colormap of the model which shows circular pattern around the source. In this model, the correlation length is constant for all incident planes. This heterogeneity geometry clearly demonstrates how the effects of fracture density heterogeneity on AVOA depend on the azimuthal angle $\phi$. In the slow wave direction ($\phi = 0°$), fracture density heterogeneity perturbs AVOA at maximum

strength, and the AVOA residue clearly recovers model heterogeneity pattern. As $\phi$ increases, the circular rings smear out. In the fast wave direction ($\phi = 90°$), the rings disappear. This test model verifies that the perturbation strength inversely depends on azimuthal angle $\phi$.

In reality the heterogeneity distribution seldom follows regular patterns such as those we have shown. Therefore, we also need to test more realistic models built with stochastic functions of the fracture density distribution.

Figure 6 shows a stochastic model where the fracture density heterogeneity distribution takes the form of a von Kármán function. The correlation lengths are 300 m in both the x and y directions. Figure 7a is a similar model with correlation lengths at 100 m in x and 300 m in y. As in the other models, the mean fracture density is 10%, with perturbations of ±5%. For these irregular patterns, we see the AVOA residues of P and SV waves do show some relationship between the large scale heterogeneous areas of model and the AVOA response. The model images, however, are severely distorted due to nonlinearities of the AVO dependence on the incident and the azimuthal angles.

# CONCLUSIONS

We use a 3-D finite-difference numerical model to more accurately simulate reflection from fractured reservoirs. We calculate AVOA, and show its dependence of the fracture density and the contrasts of elastic properties of the model layers. The results also show the sensitivity comparison of P and SV waves to the fractures. For a medium with a heterogeneous fracture density distribution, we find that the AVOA residues can be used to estimate the perturbation strength and distribution of fracture density heterogeneity in a reservoir. In processing field data, the Shuey's equation can be used to find AVOA residues.

# REFERENCES

Banik, N. C., 1987, An effective anisotropy parameter n transverserly isotropic media, *Geophysics, 52*, 1654–1664.

Hudson, J. A., 1981, Wave speeds and attenuation of elastic waves in material containing cracks, *Geophys. J. Roy. Astr. Soc., 64*, 133–150.

Hudson, J. A., 1990, Overall elastic properties of isotropic materials with arbitrary distribution fo circular cracks, *Geophys. J. Int., 102*, 465–469.

Hudson, , J. A., Liu, E., and Crampin, S., 1996a, Transmission properties of a plane fault, *Geophys. J. Int., 125, No.2*.

Hudson, , J. A., Liu, E., and Crampin, S., 1996b, The mechanical properties of materials with interconnected cracks and pores, *Geophys. J. Int., 124*, 105–112.

Mueller, M. C., 1991, Prediction of lateral variability in fracture intensity using multicomponent shear-wave surface seismic as a precursor to horizontal drilling in the Austin Chalk, *Geophys. J. Int., 1991*, 409–415.

Li, X., Kühnel, T. and MacBech, C., 1996, Mixed mode AVO response in fractured media, *SEG Expanded Abstracts, 66*, 1822–1825.

Rüeger, A., Tsvankin, I., 1995, Azimuthal variation of AVO response for fractured reservoirs, *SEG Expanded Abstracts, 65*, 1103

Sayers, C. M., Rickett, 1997, J. E., Azimuthal variation in AVO response for fractured gas sands, *Geophysical Prospecting, 45*, 165–182.

Teng, L., Mavko, G., 1996, Fracture signatures on P-wave AVOZ, *SEG Expanded Abstracts, 66*, 1818–1821.

Thomsen, L., 1993, Weak anisotropic reflections, *Offset-dependent reflectivity: Theory and practice of AVO analysis*, 103–111.
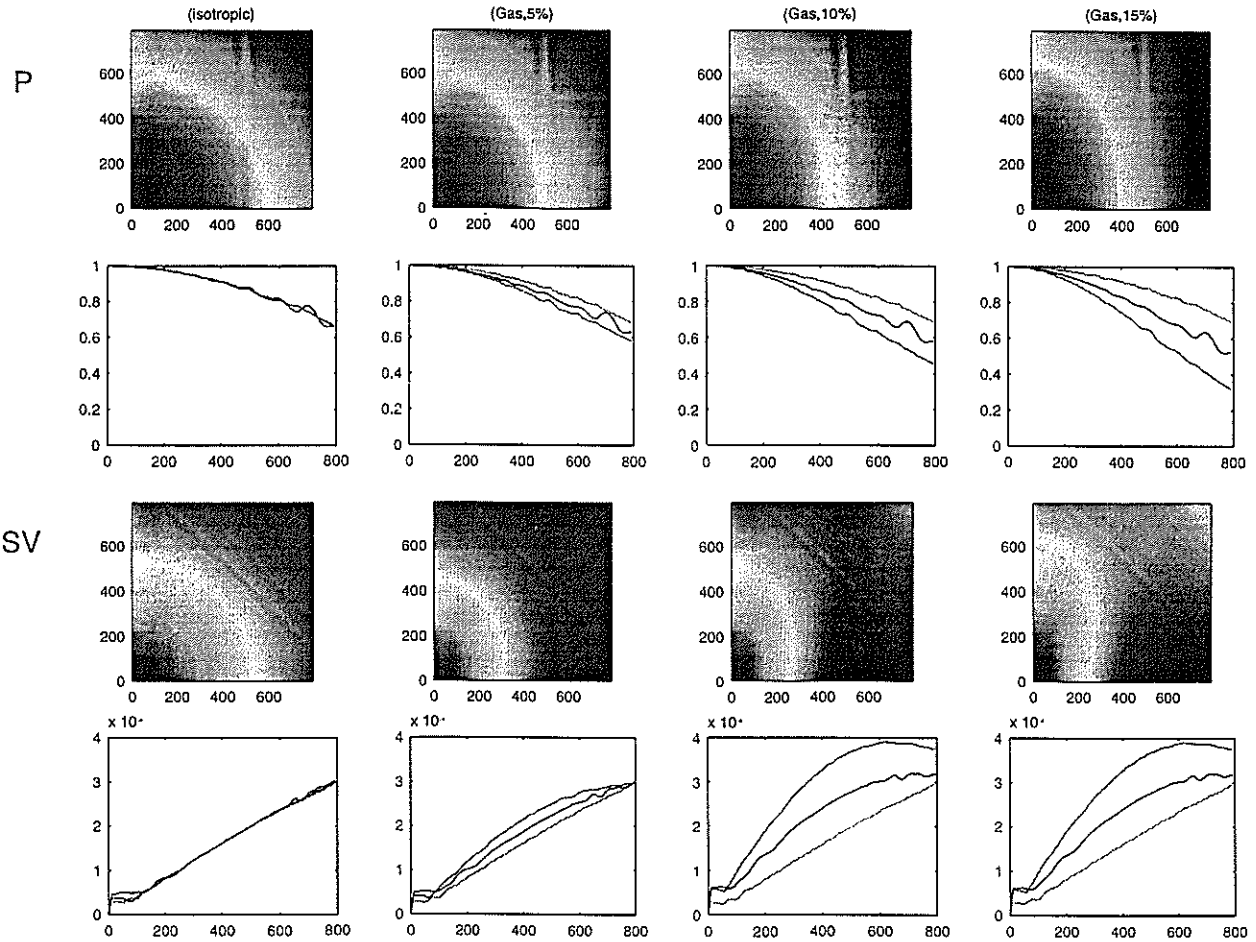
Figure 1: AVOA of P-P and P-SV waves varying with fracture density. From left to right, each column is for fracture density of 0%(isotropic), 5%, 10% and 15% respectively. The 1st row: AVOA colormap of P wave; The 2nd row: AVO curves of P waves(the maximum offset corresponds to 30° incident angle, green–$\phi = 90°$, blue–$\phi = 45°$, red–$\phi = 0°$); The 3rd row: AVOA colormap of SV wave; The 4th row: AVO curves of SV waves.
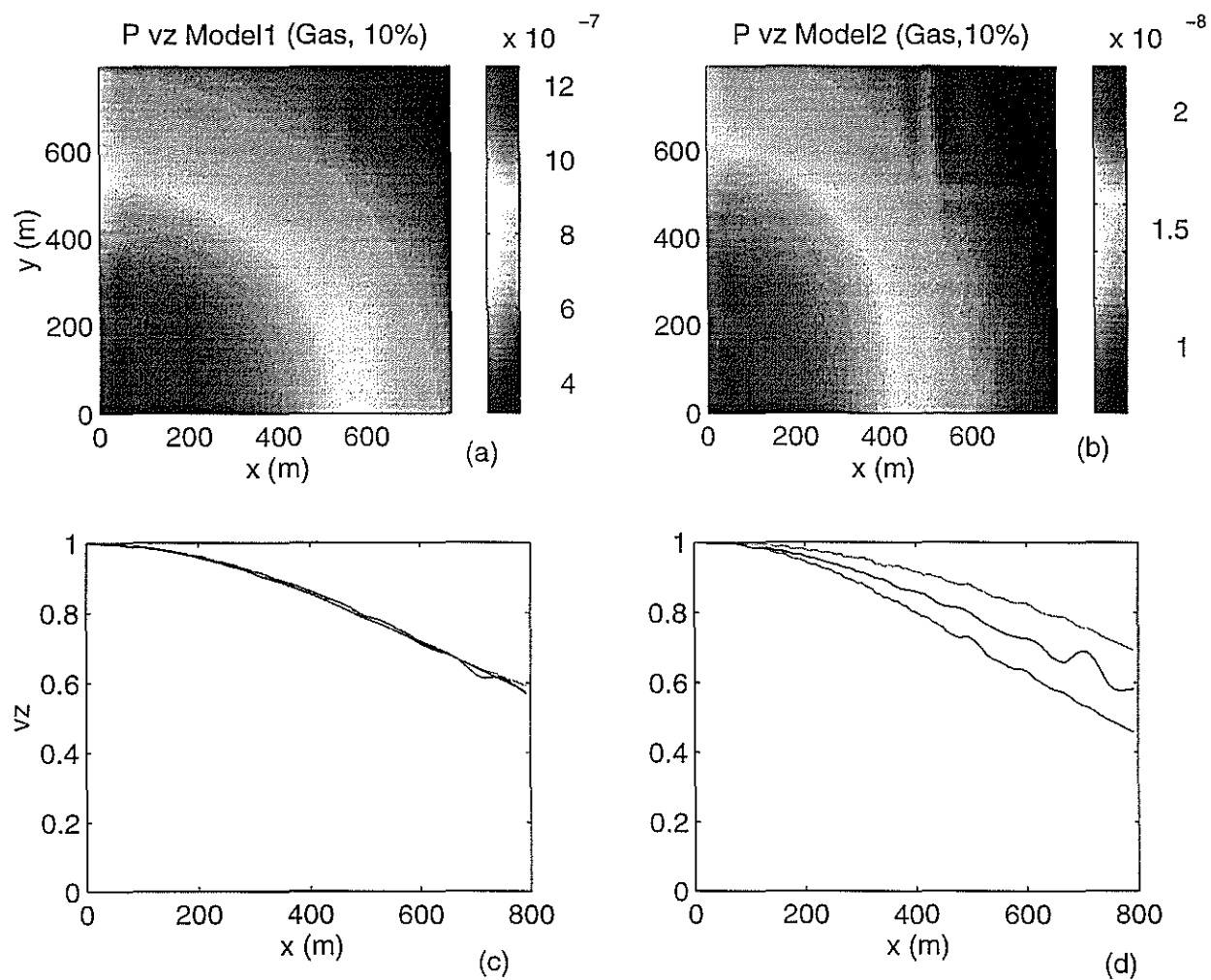
P vz Model1 (Gas, 10%)    x 10$^{-7}$

P vz Model2 (Gas,10%)    x 10$^{-8}$

(a)

(b)

(c)

(d)

Figure 2: AVOA of two models, both containing gas-saturated fractures with fracture density at 10%. The first column is for model 1, which has large velocity contrast; the second column is for model 2, in which the contrast is much smaller.
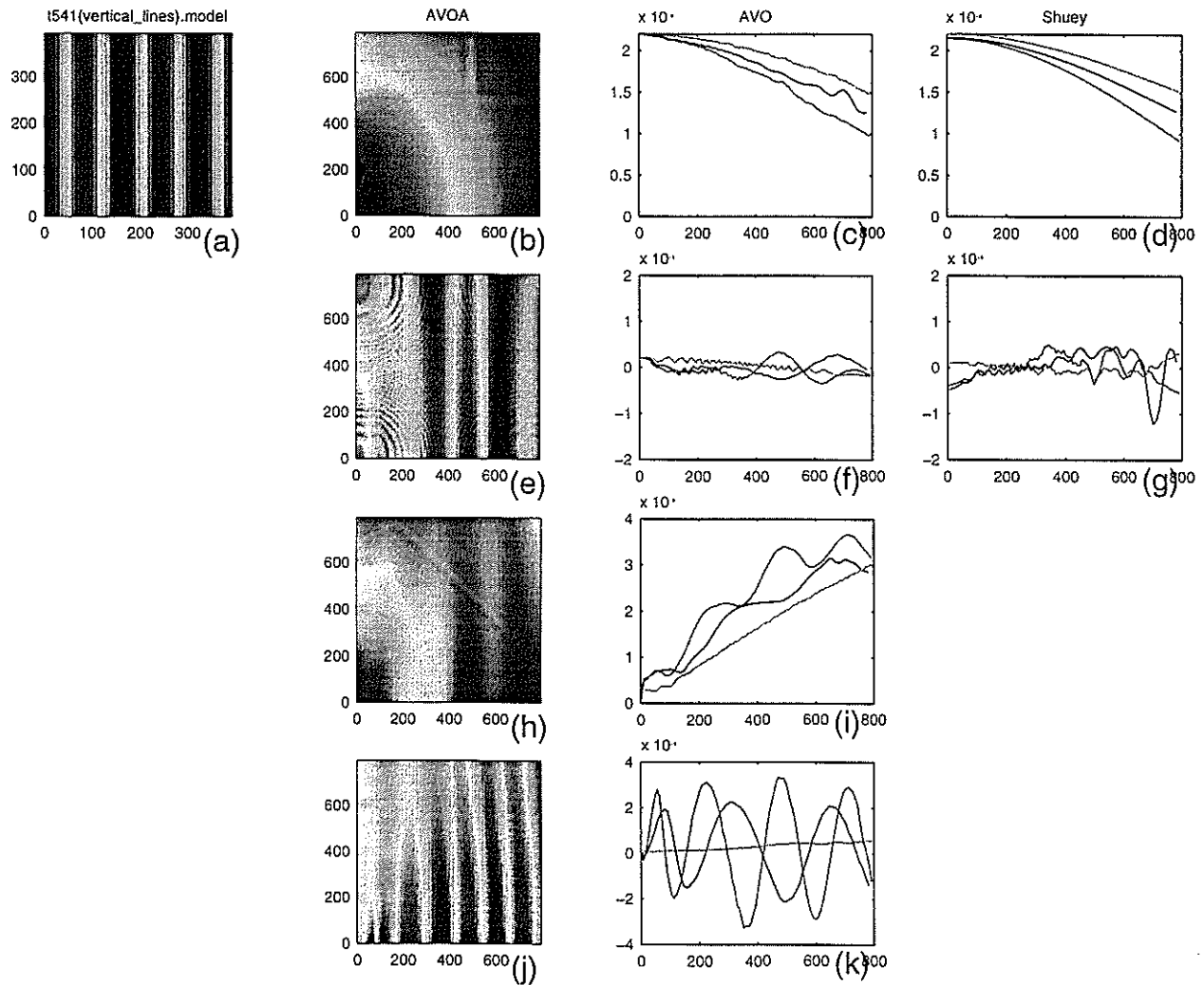
Figure 3: AVOA of heterogeneous model 1 (vertical-lines pattern). (a). The colormap of fracture density in the model reflecting area; (b). AVOA of P wave; (c). AVO curves of P wave; (d). AVO curves fitted into Shuey's equation; (e). AVOA residue (homogeneous background removed); (f). AVO curves residues; (g). AVO residues after removing Shuey's equation; (h). AVOA of SV wave; (i). AVO curves of SV wave; (j). AVOA residue of SV wave; (k). AVO curves residues.
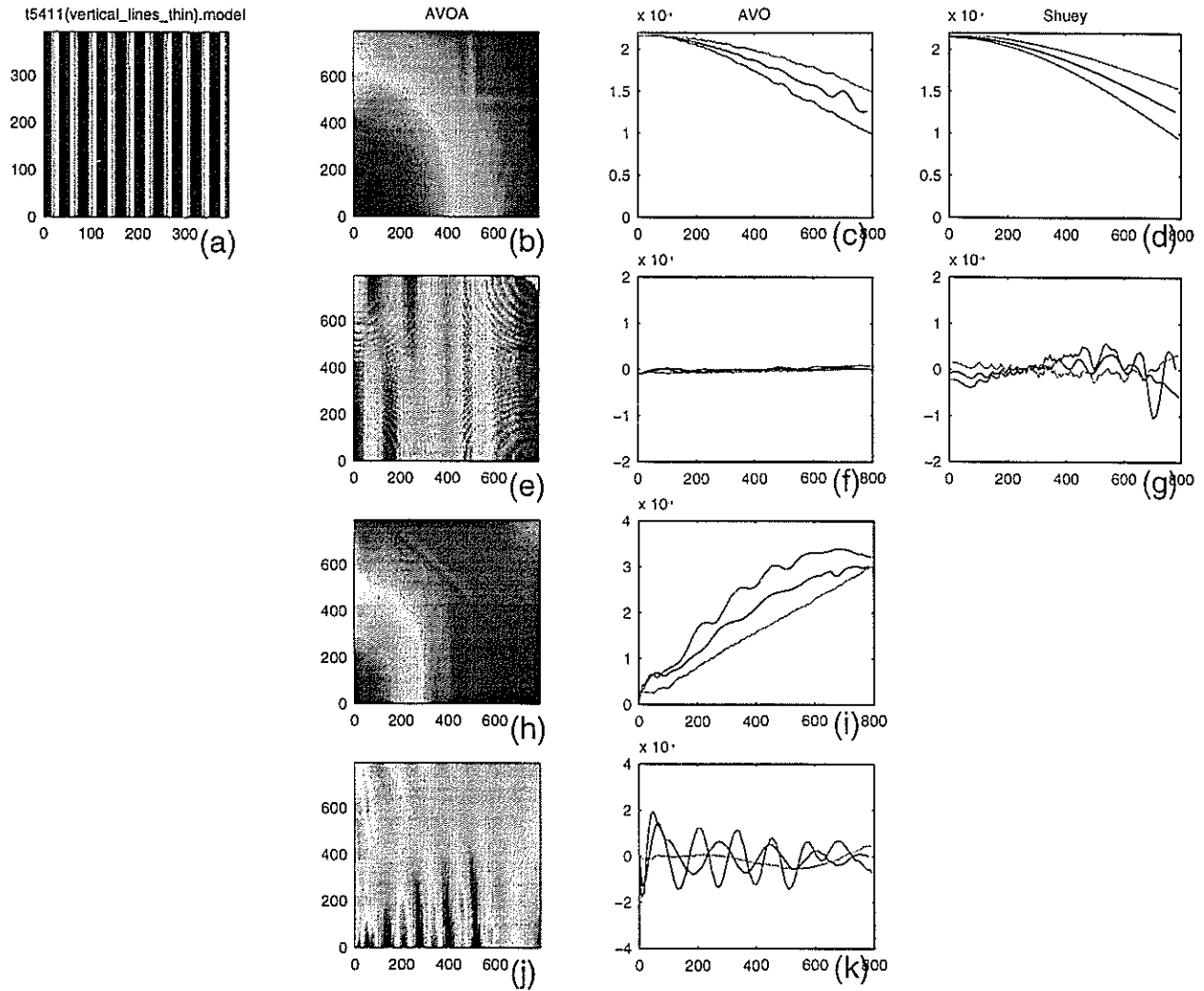
Figure 4: AVOA of heterogeneous model 3 (thin-vertical-lines pattern). (a). The colormap of fracture density in the model reflecting area; (b). AVOA of P wave; (c). AVO curves of P wave; (d). AVO curves fitted into Shuey's equation; (e). AVOA residue (homogeneous background removed); (f). AVO curves residues; (g). AVO residues after removing Shuey's equation; (h). AVOA of SV wave; (i). AVO curves of SV wave; (j). AVOA residue of SV wave; (k). AVO curves residues.
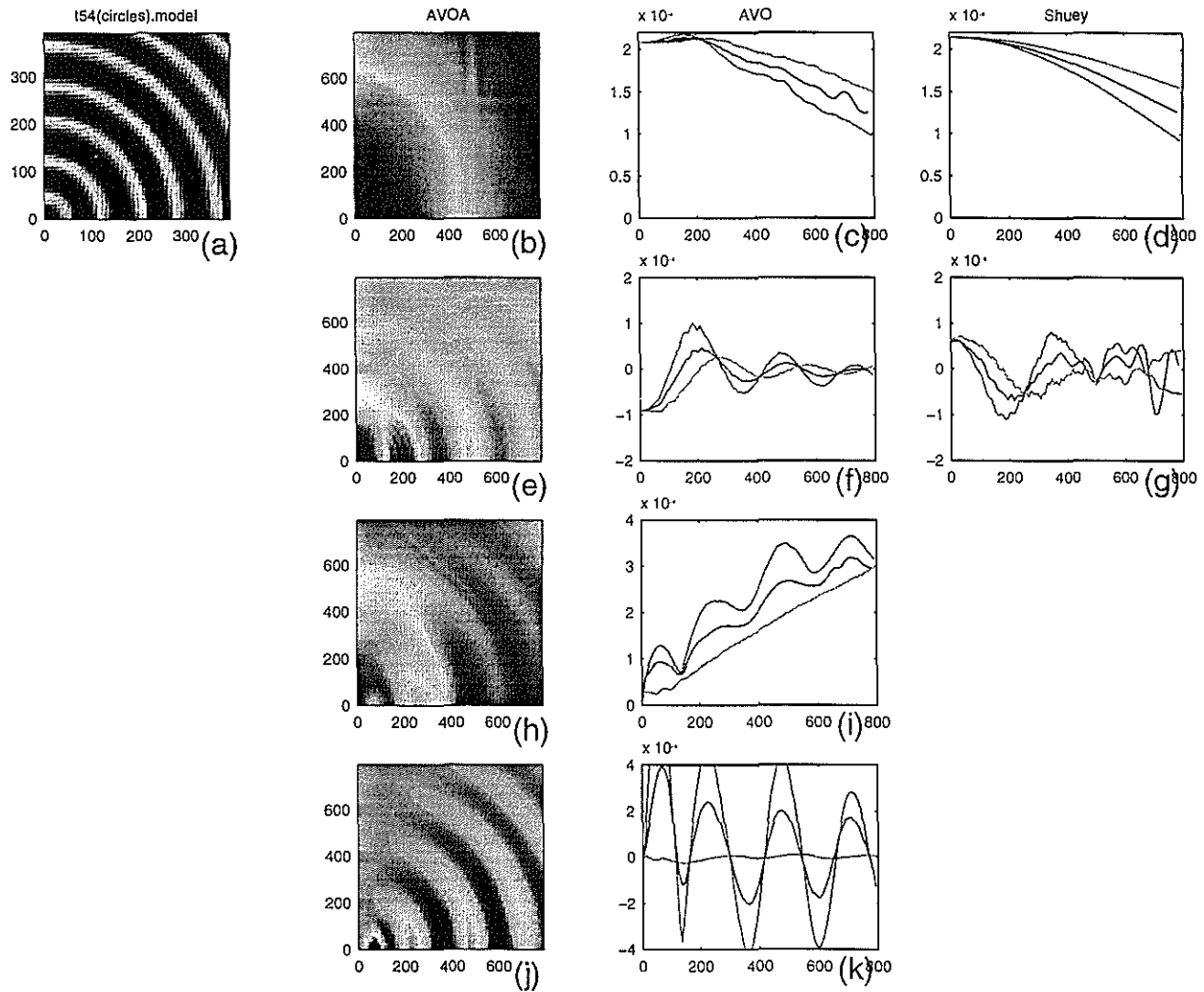
Figure 5: AVOA of heterogeneous model 4 (circles pattern). (a). The colormap of fracture density in the model reflecting area; (b). AVOA of P wave; (c). AVO curves of P wave; (d). AVO curves fitted into Shuey's equation; (e). AVOA residue (homogeneous background removed); (f). AVO curves residues; (g). AVO residues after removing Shuey's equation; (h). AVOA of SV wave; (i). AVO curves of SV wave; (j). AVOA residue of SV wave; (k). AVO curves residues.
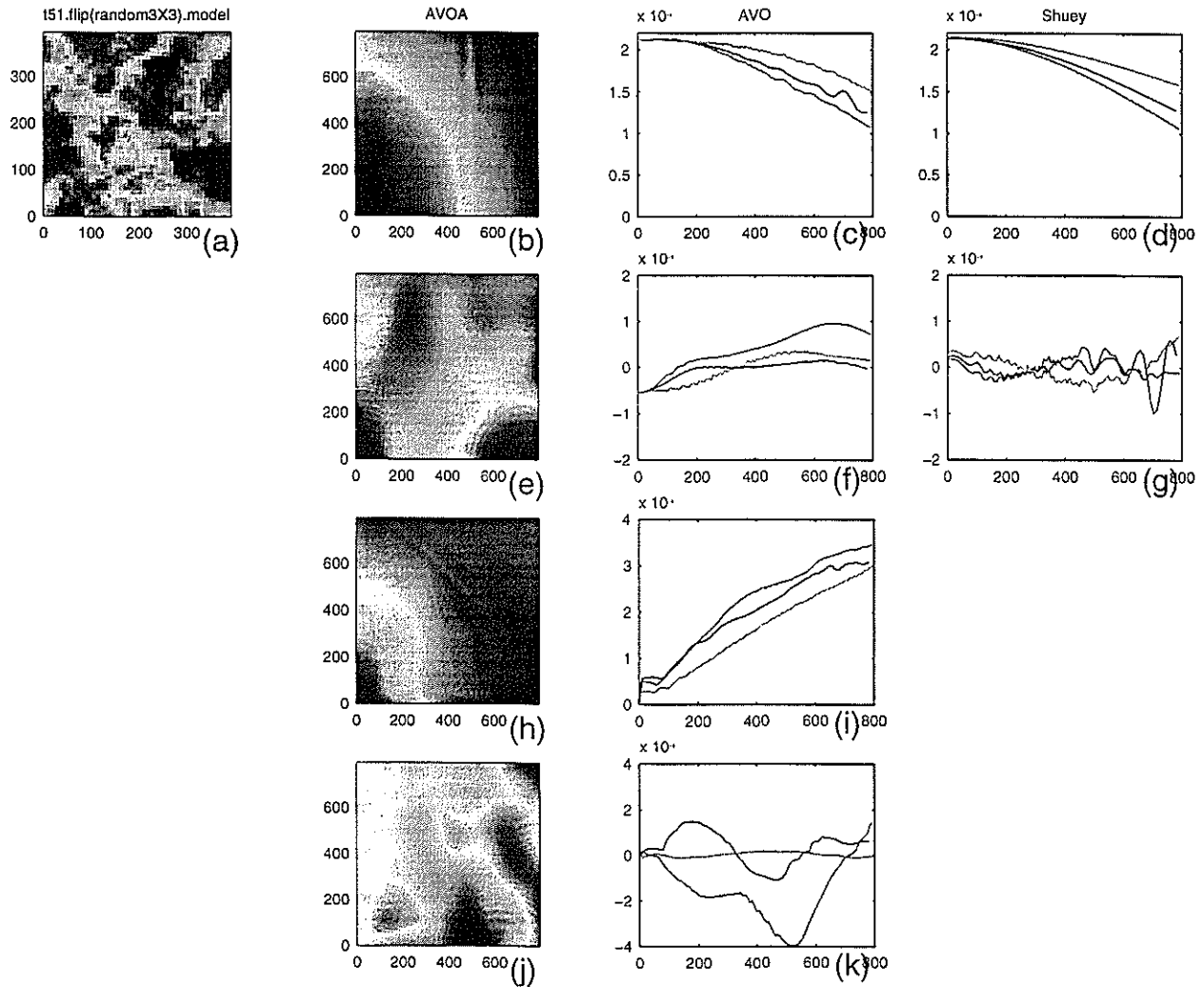
Figure 6: AVOA of heterogeneous model 6 (von Kármán, 3X3). (a). The colormap of fracture density in the model reflecting area; (b). AVOA of P wave; (c). AVO curves of P wave; (d). AVO curves fitted into Shuey's equation; (e). AVOA residue (homogeneous background removed); (f). AVO curves residues; (g). AVO residues after removing Shuey's equation; (h). AVOA of SV wave; (i). AVO curves of SV wave; (j). AVOA residue of SV wave; (k). AVO curves residues.
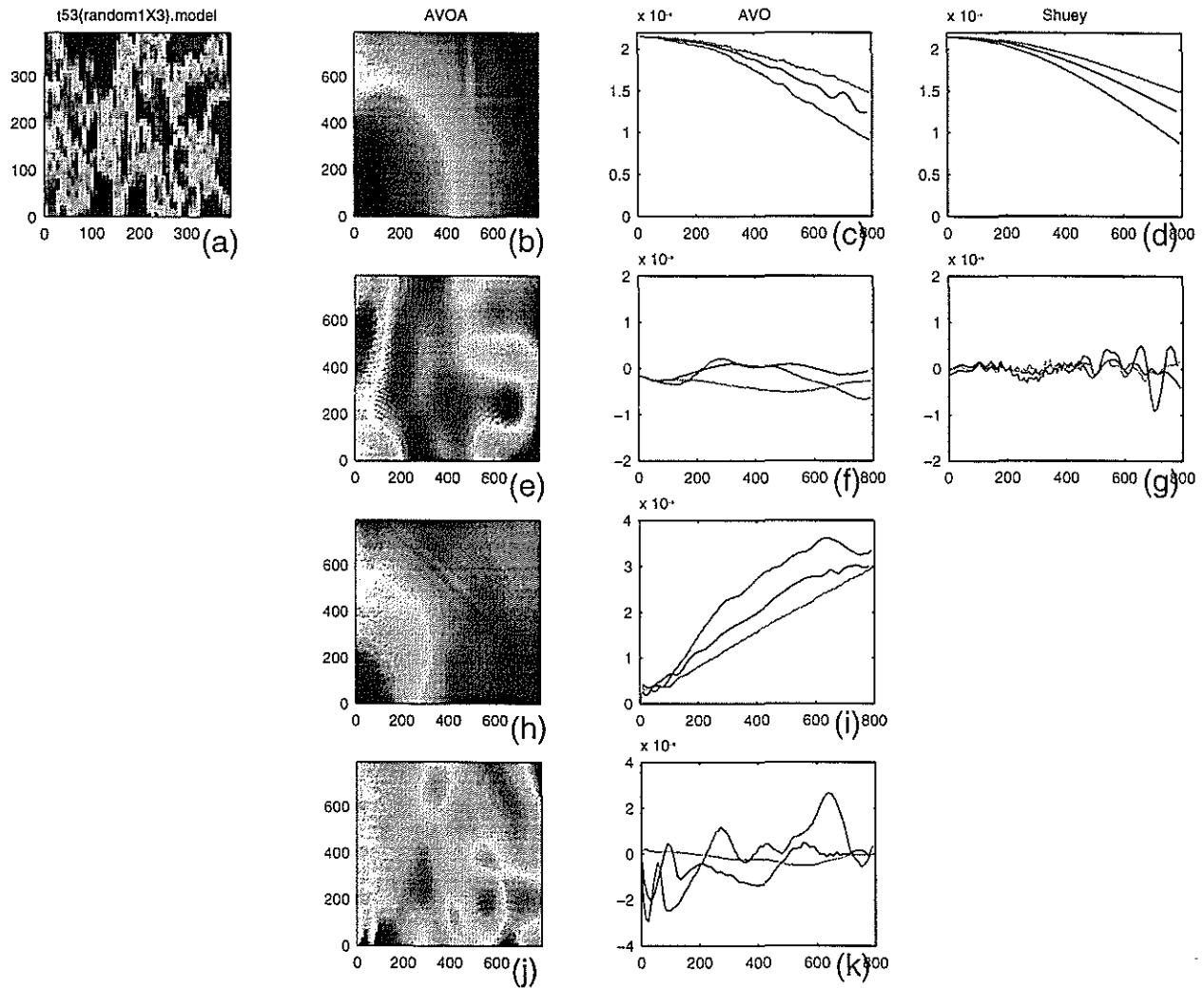
Figure 7: AVOA of heterogeneous model 7 (von Kármán, 1X3). (a). The colormap of fracture density in the model reflecting area; (b). AVOA of P wave; (c). AVO curves of P wave; (d). AVO curves fitted into Shuey's equation; (e). AVOA residue (homogeneous background removed); (f). AVO curves residues; (g). AVO residues after removing Shuey's equation; (h). AVOA of SV wave; (i). AVO curves of SV wave; (j). AVOA residue of SV wave; (k). AVO curves residues.